Frontiers in Heat and Mass Transfer (FHMT), 9, 28 (2017)
DOI: 10.5098/hmt.9.28

Global Digital Central
ISSN: 2151-8629

Frontiers in Heat and Mass Transfer

Available at www.ThermalFluidsCentral.org

MRT-LBM SIMULATION OF NATURAL CONVECTION IN A RAYLEIGH-BENARD CAVITY WITH LINEARLY VARYING TEMPERATURES ON THE SIDES: APPLICATION TO A MICROPOLAR FLUID

A. El Mansouri[a-b], M. Hasnaoui[a,*], A. Amahmid[a], Y. Dahani[a], M. Alouah[a], S. Hasnaoui[a], R. Khaoula[a], M. Ouahas[a] and R. Bennacer[b]

[a]*UCA, Faculty of Sciences Semlalia, Physics Department, LMFE, Unit affiliated to CNRST (URAC 27), BP 2390, Marrakech, Morocco*

[b]*ENS-Cachan Dpt GC/LMT, 61, Av du Président Wilson 94235 Cachan Cedex France*

ABSTRACT

A two-dimensional numerical simulation is conducted to study natural convection flow and heat transfer characteristics in a square cavity filled with a micropolar fluid. The lower and upper walls of the cavity are respectively subject to isothermal heating and cooling while the temperatures of both vertical sides decrease linearly in the upwards direction. The Lattice-Boltzmann Method (LBM), with the multi-relaxation time (MRT) scheme for the collision process, is used to solve the problem with the objective to assess the ability and efficiency of this numerical method to describe the micropolar fluid behavior under the effect of the imposed thermal boundary conditions. Computations are carried out for Rayleigh number, Ra, and material parameter (vortex viscosity), K, varying respectively in the ranges $10^3 \leq Ra \leq 10^6$ and $0 \leq K \leq 2$. Combined effects of these parameters on the multiplicity of solutions and critical values of Ra from which transitions occur are investigated for $\Pr = 7$. An increase of the material parameter K is shown to increase the critical Rayleigh numbers, which confirms the stabilizing effect of the micropolar fluid compared to the Newtonian case ($K = 0$). The study covers both steady and unsteady aspects of the problem under consideration. Initial perturbations play an important role in the cooling process of the hot bottom wall in the present configuration. The bicellular ascending and descending flows are two solutions mirror images of each other but they lead to very different quantities of heat from the bottom wall.

Keywords: *Steady & unsteady natural convection, MRT-LBM, Micropolar fluid.*

1. INTRODUCTION

Natural convection is the most important mode of heat exchange in several industrial devices and engineering applications involving fluids. Solar collectors, heat storage systems and cooling of electronic components are some examples, among many others, where convection plays a key role in the heat evacuation process. Thereby, an extensive number of papers have been produced through the decades on natural convection phenomenon experimenting various geometries under the effect of different kinds of thermal boundary conditions (Bénard, 1900; Ostrach, 1972; Hasnaoui et *al.*, 1992; Saha, 2011). Nowadays, natural convection is still widely studied in closed cavities because this basic configuration provides a useful basis for widespread applications in many fields (Bejan, 2004; Aounallah et *al.*, 2013). The earlier results presented by De Vahl Davis (1983) in an air-filled cavity submitting to a differential heating indicate that the flow structure is monocellular and the steady-regime in such a configuration is quickly reached. On the contrary, the study of Rayleigh-Bénard convection is more complex. In fact, the origin of this complexity is attributed to the occurrence of many levels of instabilities (onset of convection, transitions towards single and multiple periodic regimes, transition towards chaotic regimes ...) and eventual existence of multiplicity of solutions, characterized by their ranges of existence and different transitions normally observed at the limit of these ranges (see for instance (Mansour et *al.*, 2006; Khadiri et *al.,* 2010)). Heat transfer improvement or deterioration depends strongly[1] on the shape of the confining configuration and the imposed boundary conditions, whose combination control the generated flow structure and temperature distribution within the systems under study. Although the phenomenon of Rayleigh-Bénard convection in rectangular configurations was the subject of many previous works (Pallares et *al.*, 1999; Calgagni et *al.*, 2005; Kao and Yang, 2007; Platten et *al.*, 2007, Raji et *al.*, 2013), the topic remains an attractive field of investigation. In fact, further understanding of the system behaviors are required, mainly, when thermal excitations on the sidewalls are changed from adiabatic or periodic conditions to linear imposed temperatures. Furthermore, for the majority of investigations related to buoyancy driven flows, the working fluids are considered Newtonian, whose behaviors are described by the well-established Navier-Stokes and energy equations. As known, the formulation of these equations is based on the classical continuum theory that neglects some characteristics of real fluids such as deformation, viscoelasticity or rotation of particles, which makes the mathematical formulation easy and the computation of fluid dynamics very approachable. The literature review shows however that many researchers have focused their efforts to build up new models and

* *Corresponding author. Email: hasnaoui@uca.ac.ma*

Global Digital Central
ISSN: 2151-8629

theories offering better descriptions of the physical genuineness of the resulting phenomena of some emergent fluids such as micropolar fluids.

In the theory of micropolar fluids, introduced earlier by Eringen (1966,1972), some corrective terms are added to the classical Navier-Stokes model in addition to a new equation specific to this kind of fluids, which contain particles of microscopic size. This theory, based on the local effects arising from microstructures and intrinsic motions of the fluid elements, once considered, is expected to describe effectively the non-Newtonian behavior of many fluids (polymers, liquid crystals, colloidal fluids, ferro liquids, suspension solutions, animal bloods, liquid with polymer additives, etc.). Under the shear stress applied on particles present in these fluids, the former (particles) can rotate about their own axis. This proper rotation, commonly known micro-rotation, should be considered by adding a new conservation equation (angular momentum equation) coupled with the slightly modified Navier-Stokes equations. Thus, this new formulation ensures a significant coupling between the self-spinning motion induced by gyration and the velocity field in the fluid domain. The first experimental study dedicated by Hoyt and Fabula (1964) to investigate this class of fluids with suspensions, has shown a significant reduction in terms of flow velocity (up to 30% of velocity attenuation) by comparison with classical fluids (those without suspensions). This reduction of velocity is due to the presence of self-spinning particles in the basic fluid which induces an increase of its effective viscosity. Lukaszewicz (1999) gives more information on the mathematical theory of the equations modelling micropolar fluids and some applications involving these fluids.

Investigations on convection concerning non-Newtonian fluids confined in cavities of various shapes is obviously sparse compared to the impressive number of works dedicated to the Newtonian case. The existing works on micropolar fluids have been generally devoted to investigate the effect of microstructures on thermal convection keeping in mind the results of the Newtonian case as a reference. In an earlier study, Jena and Bhattacharyya (1986) studied numerically, with the finite element method (Galerking method), the effect of microstructures on thermal convection in a rectangular box heated from below. They concluded that the micropolar fluid plays a stabilizing role, since the corresponding computed critical Rayleigh number was found to be higher than that of a Newtonian fluid. Few years later, Hsu et al. (1996) investigated numerically, with the aid of the cubic spline collocation method, natural convection of a micropolar fluid confined within a square cavity heated from below. They showed that, compared to the Newtonian fluid, heat transfer undergoes a deterioration and the onset of thermal convection is delayed in the case of fluids with microstructures. Hsu et al. (1997) studied numerically natural convection in a tilted enclosure equipped with a single or multiple uniform heat sources. The effect of arrangements and locations of the latter on heat transfer has been investigated with the objective to attain qualitative suggestions that may help to improve the cooling design of the system. Comparative results of thermal and dynamic characteristics of Newtonian and micropolar fluids have shown smaller heat transfer and flow velocities in the case of micropolar fluids. The numerical study conducted by Aydin and Pop (2007) on micropolar fluids confined within a differentially heated cavity has focused on the search of optimal combinations of the governing parameters has showed the meaningful effect of micro-particles presence on heat transfer flow. Recent studies on micropolar fluids (Koriko and Animasaun, 2017; RamReddy and Pradeepa, 2017; Miroshnichenko et *al.*, 2017), all based on digital tools, have shown that the micro-rotation has a significant effect on thermal and flow characteristics and thereby, this parameter should be considered for the design of cooling systems where gravity acts as a driving force.

To the best of the authors' knowledge, only classical methods have been used in the previous studies that have addressed numerically the micropolar fluids. Recently, the lattice-Boltzmann method (LBM) has experienced unprecedented success in simulating fluid flows and associated transport phenomena. In addition, the LBM has attracted attention because of its easy implementation to deal with complex problems. In the meantime, compared to CFD methods used to explore problems involving fluid flows and heat transfer, this method provides the possibility of parallel coding and it is flexible in the treatment of irregular boundaries in complex geometries. Moreover, the LBM has been experimented successfully and seems to be a powerful tool for simulating problems such as melting (Huber et *al.*, 2008), flows in porous media (Guo and Zhao, 2005), and nanofluids (Nemati et *al.*, 2010, Mliki et *al.*, 2016; El Abdallaoui et *al.*, 2015).

The aim of the present paper is to extend the LBM to investigate natural convective heat transfer of micropolar fluids confined in a Rayleigh-Bénard configuration with imposed linear temperatures on its sidewalls. The study focuses on the effect of the main governing parameters on the multiplicity of solutions, the existence ranges of the latter and the different transitions occurring in such problems. Quantitative and qualitative comparisons with the Newtonian fluids are presented in terms of streamlines, isotherms and heat transfer characteristics.

2. Mathematical formulations

The studied configuration is a square cavity heated from below, cooled from above and subjected to a linear variation of the temperature from the sidewalls (Fig. 1). The cavity is filled with a micropolar fluid composed of a base fluid with a Prandtl number equal 7 but containing particles of microscopic size and characterized by the vortex viscosity parameter K. The physical properties of the base fluid are considered constant with the exception of the density in the buoyancy term. The study is conceived 2D with the assumption of laminar and incompressible flow. The governing equations of the problem are described in previous works (see for instance (Aydin and Pop, 2007)).

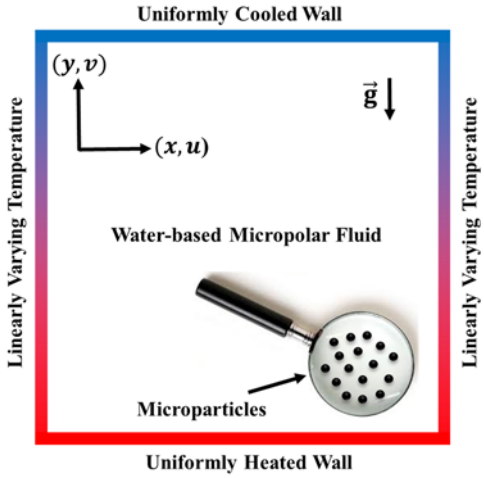

Fig. 1 Physical problem with thermal boundary conditions.

The dimensionless form of the problem, based on the vorticity-stream function formulation, is obtained by scaling length, time, velocity, temperature and micro-rotation respectively by L, L^2/α, L/α, $\Delta T=T_h-T_c$, and α/L^2:

$$\frac{\partial \Omega}{\partial \tau} + \nabla.(V\Omega) = Pr(1+K)\Delta\Omega - PrK\Delta\Phi + PrRa\frac{\partial \theta}{\partial X} \quad (1)$$

$$\frac{\partial \theta}{\partial \tau} + \nabla.(V\theta) = \Delta\theta \quad (2)$$

$$\frac{\partial \Phi}{\partial \tau} + \nabla.(V\Phi) = Pr\left(1+\frac{K}{2}\right)\Delta\Phi + PrK(\Omega - 2\Phi) \quad (3)$$

Where Ω, $Pr = \upsilon/\alpha$, $Ra = g\beta\Delta TL^3/\upsilon\alpha$ and $K = \kappa/\mu$ are respectively the vorticity, the Prandtl number, the Rayleigh number, and the vortex viscosity.

Global Digital Central
ISSN: 2151-8629

The corresponding initial and boundary conditions are as follows:
Initial conditions corresponding to the rest state at $\tau = 0$:

$$V = \psi = \Phi = \theta = 0 \qquad \text{for } 0 \le X, Y \le 1 \tag{4}$$

For $\tau > 0$:

$$\begin{aligned} V = \psi &= 0 && \text{on the rigid boundaries} \\ \theta = \theta_h = 1 \text{ and } \Phi &= -\eta \frac{\partial V_x}{\partial Y} && Y = 0 \text{ and } 0 \le X \le 1 \\ \theta = \theta_c = 0 \text{ and } \Phi &= -\eta \frac{\partial V_x}{\partial Y} && Y = 1 \text{ and } 0 \le X \le 1 \\ \left.\begin{aligned} \theta &= \theta_h - (\theta_h - \theta_c)Y \\ \Phi &= -\eta \frac{\partial V_y}{\partial X} \end{aligned}\right\} & && X = 0, 1 \text{ and } 0 \le Y \le 1 \end{aligned} \tag{5}$$

where η is a parameter that may vary between 0 and 1. The present study is restricted to the case $\eta = 0$ which corresponds to a strong concentration of the micro-particles near the walls. This high concentration of microparticles consequently prevents their ability to rotate ($\Phi = 0$). The case $\eta = 1/2$, corresponds to the vanishing of the stress tensor anti-symmetric part and denotes a weak concentration. The case $\eta = 1$ may be used for modeling the turbulent boundary layer flows (Aydin and Pop, 2007).

3. The Lattice-Boltzmann method

3.1 D2Q9 model for fluid flow

The use of the Lattice-Boltzmann method to simulate fluid dynamics has become very popular during these last years. This method is specifically based on the resolution of the following Lattice-Boltzmann equation initially derived from Lattice-Gaz-Automota (LGA):

$$f(r + c\Delta t, t + \Delta t) - f(r, t) = \mathbb{C}(f) \tag{6}$$

where f is the distribution function of a particle with velocity $c = (c_x, c_y)$ at time t and location $r = (x, y)$. The left-hand part of Eq. (6) represents the propagation process while $\mathbb{C}$ is the collision operator.
The values of discrete velocities corresponding to D2Q9 model, sketched in Fig. 2a, are giving by:

$$(c_x, c_y) = \begin{cases} (0,0) \;\; / \;\; k = 0 \\ \left(\cos\left(\frac{(k-1)\pi}{2}\right), \sin\left(\frac{(k-1)\pi}{2}\right)\right) c \;\; / \; 1 \le k \le 4 \\ \left(\cos\left(\frac{(2k-9)\pi}{4}\right), \sin\left(\frac{(2k-9)\pi}{4}\right)\right) c \;\; / \; 5 \le k \le 8 \end{cases} \tag{7}$$

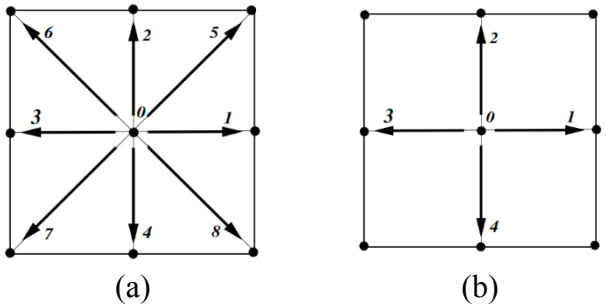

Fig. 2 The two-dimensional D2Q9 velocity (a) and D2Q5 temperature and micro-rotation (b) models.

The fluid is perceived as a set of particles moving on a regular lattice of $N \times N$ nodes (the lattice spacing is set to unity $\Delta x = \Delta y = 1$), where N is the number of nodes considered in each of x and y directions of the square cavity. At each time step ($\Delta t = 1$), particles propagate towards the neighboring nodes with velocity $c = \frac{\Delta x}{\Delta t} = \frac{\Delta y}{\Delta t}$ and redistribute their velocities in a local collision. In this work, the collision process is modeled by a multi-relaxation time scheme (MRT) which has the advantage of being more accurate than the simple-relaxation time scheme (SRT). In addition, this model improves the numerical stability and reduces the non-physical oscillations (Lallemend and Luo, 2000; Qian et *al.*, 1992) in comparison with the simple single relaxation time scheme based on the Bhatnagar, Gross and Krook (BGK) approximation (Wu and Shao, 2004). In the MRT scheme, the streaming phase is performed in the microscopic space defined by a set of nine discrete velocities as illustrated in Fig. 2a with distribution functions $f = \{ f_k \mid 0 \le k \le 8\}$ while the collision phase is handled in the moment space $m = \{ m_k \mid 0 \le k \le 8\}$ constructed based on the moments of f_k. Qian *et al.* (1992) defined a transformation matrix M that allows the mapping between the two spaces as follows:

$$m = Mf \tag{8}$$

The nine components of the moment vector, m, and the matrix M are given with their physical signification in the reference (Bouzidi et *al.*, 2001).

In the absence of a body force, three macroscopic moments are conserved (those corresponding to mass and momentum conservation) during the collision process, we can write:

$$m_0^* = m_0 = \rho \tag{9}$$

$$m_3^* = m_3 = j_x \tag{10}$$

$$m_5^* = m_5 = j_y \tag{11}$$

The symbol '*' denotes the post-collision moments. In natural convection, the buoyancy driven force acting on the fluid modifies the momentum. Thus, the x-component F_x and the y-component F_y of the buoyancy force $F = \rho g \beta(\theta - \theta_0)$ should be added to the right-hand parts of equations (10) and (11), respectively. The temperature $\theta_0 = (\theta_h + \theta_c)/2$ is the mean temperature of the fluid. The effect induced by the spinning of the micro-particles on the fluid flow is considered by adding source terms to conservation equations of momentum (see the above equations). In the same way, these source terms are added to the right-hand parts of equations (10) and (11) which become:

$$m_3^* = m_3 + F_x + \frac{\kappa}{\rho}\frac{\partial \phi}{\partial y} = m_3 + F_x + {\upsilon_l}^2 \frac{K}{Pr {L_l}^2}\frac{\partial \Phi}{\partial y} \tag{12}$$

$$m_5^* = m_5 + F_y - \frac{\kappa}{\rho}\frac{\partial \phi}{\partial x} = m_5 + F_y - {\upsilon_l}^2 \frac{K}{Pr {L_l}^2}\frac{\partial \Phi}{\partial x} \tag{13}$$

Furthermore, the kinematic viscosity representing the diffusion coefficient in the Newtonian case turns to an effective viscosity $\upsilon_{eff} = \upsilon_l(1 + K/2)$ that depends on the lattice kinematic viscosity υ_l and the dimensionless vortex viscosity parameter K characterizing the microplar fluid. Hence, the relaxation parameters of the D2Q9 model are calculated using the previous effective viscosities. The lattice kinematic viscosity is habitually selected between 0.01 and 0.001 (Mohamad and Kuzmin, 2010). To avoid eventual non-physical instabilities, this parameter is expressed for natural convection and low Mach number (incompressible flows) Ma by the following expression (El Abdallaoui et *al.*, 2014):

$$\upsilon_l = \sqrt{\frac{Ma^2 N^2 Pr}{3Ra}} \tag{14}$$

Global Digital Central
ISSN: 2151-8629

For non-conserved moments, the collision process is expressed by the following equation where the moments relax to reach the equilibrium state as follows:

$$m_k^* = m_k - s_k\left(m_k - m_k^{eq}\right) \tag{15}$$

$S = diag\{s_k \mid k = 0, \dots, 8\}$ is the diagonal relaxation matrix where $s_0 = s_3 = s_5 = 0$ (correspond to the conserved moments). For pure numerical stability reasons, the rest of relaxation rates must be chosen between 0 and 2. Furthermore, s_1, s_2, s_4 and s_6 are taken slightly superior to 1 and $s_7 = s_8 = 1/(0.5 + \upsilon_{eff}/\Delta t c_s^2)$ where c_s is the sound speed of the lattice equal to $c/\sqrt{3}$ for the D2Q9 model.

The equilibrium state of the non-conserved moments is given in terms of conserved moments as follows (Mezrhab et *al.*, 2004):

$$\left.\begin{aligned} m_1^{eq} = e_{eq} &= 2(3c_s^2 - 2)\rho + 3\,(j_x^2 + j_y^2)/\rho \\ m_2^{eq} = \varepsilon_{eq} &= \rho - 3\,(j_x^2 + j_y^2)/\rho \\ m_4^{eq} = q_{x_{eq}} &= -j_x \\ m_6^{eq} = q_{y_{eq}} &= -j_y \\ m_7^{eq} = p_{xx_{eq}} &= (j_x^2 - j_y^2)/\rho \\ m_8^{eq} = p_{xy_{eq}} &= j_x j_y/\rho \end{aligned}\right\} \tag{16}$$

The assumption of incompressible flow, valid for a small Mach number ($Ma = u/c_s < 0.3$), means that the fluid density varies slowly in the fluid domain. This allows to consider the density constant, $\rho = \rho_0$, in the calculation of equilibrium moments.

Before the streaming phase, the distribution function vector f is derived from the post collision moment vector m as follows:

$$f_k\left(x + c_{x,k}\Delta t, y + c_{y,k}\Delta t, t + \Delta t\right) = f_k(x, y, t)\,, \quad 0 \le k \le 8 \tag{18}$$

The macroscopic velocities (u, v) are obtained from the distribution functions or their moments as following:

$$u = \frac{1}{\rho}\sum_{k=0}^{8} f_k . c_{x,k} = \frac{m_3}{m_1} \tag{19}$$

$$v = \frac{1}{\rho}\sum_{k=0}^{8} f_k . c_{y,k} = \frac{m_5}{m_1} \tag{20}$$

It is to be noticed that the obtained velocities and lattice time need to be scaled using the lattice thermal diffusivity $\alpha_l^\theta = \upsilon_l/Pr$ and the characteristic length $L_l = (N-1)\Delta x$, respectively.

The distribution functions, pointing inside the cavity, streamed from outside the fluid domain, reason why they are considered unknown. These functions are determined using the classical bounce-back boundary conditions.

3.2 D2Q5 model for temperature and microrotation

The D2Q5 model, used for temperature and micro-rotation, is sketched in Fig. 2b. A same gait is followed in this section to compute temperature and micro-rotation fields. The use of the D2Q5 model instead of the D2Q9 was with the objective to reduce the computational effort generally excessive for the MRT scheme. The effectiveness of the D2Q5 model was confirmed in many previous works (Mezrhab et *al.*, 2010; Guo et *al.*, 2010). In the present work, a triple distribution function (TDF) is tested to simulate velocity, temperature and micro-rotation. The TDF results are validated against those obtained with a finite difference method by solving Eqs. (2) to (3) with the associated initial and boundary conditions, Eqs. (4) and (5). Thus, we define $g = \{g_k | k = 0, \dots, 4\}$ and $h = \{h_k | k = 0, \dots, 4\}$ as the distribution function vectors related, respectively, to temperature and microrotation in the discrete velocity space. For each of these function vectors, there exists a vector of moments in the moment space defined by:

$$m^\theta = M'g \qquad \text{and} \qquad m^{\mathbf{\Phi}} = M'h \tag{21}$$

In the precedent relations, M' is a 5×5 matrix that transforms g and h to m^θ and m^Φ, given as follows:

$$M' = \begin{pmatrix} 1 & 1 & 1 & 1 & 1 \\ 0 & 1 & 0 & -1 & 0 \\ 0 & 0 & 1 & 0 & -1 \\ -4 & 1 & 1 & 1 & 1 \\ 0 & 1 & -1 & 1 & -1 \end{pmatrix}$$

During the collision process, the non-conserved moments relax at different rates to reach the equilibrium state according to the following relation:

$$m_k^{I,*} = m_k^I - s_k^I\left(m_k - m_k^{I,eq}\right), \qquad k = 1, \dots, 4 \tag{22}$$

where I stays for temperature θ or microrotation Φ, $s_1^\theta = s_2^\theta = \left(\frac{10\alpha_l^\theta}{4+a} + 0.5\right)^{-1}$ and $s_1^\Phi = s_2^\Phi = \left(\frac{10\alpha_l^\Phi}{4+a} + 0.5\right)^{-1}$ are relaxation rates depending on the thermal diffusivity, α_l^θ and the diffusion coefficient related to micro-rotation equation, $\alpha_l^\Phi = \upsilon_l(1 + K)$. The constant a is set to -2 in order to have the same sound speed in both D2Q9 and D2Q5 models.

The following relations provide the corresponding equilibrium moments:

$$\left.\begin{aligned} m_0^{I,eq} &= I \\ m_1^{I,eq} &= uI \\ m_2^{I,eq} &= vI \\ m_3^{I,eq} &= aI \\ m_4^{I,eq} &= 0 \end{aligned}\right\} \tag{23}$$

The temperature field is derived from the conserved moment. The latter is amended in the case of micro-rotation by a source term expressing the strong coupling between the velocity field and the spin of micro-particles present in the fluid:

$$\left.\begin{aligned} \theta &= m_0^\theta = \textstyle\sum_{k=0}^4 g_k \\ \Phi &= m_0^\Phi + Q = \textstyle\sum_{k=0}^4 h_k + Q \end{aligned}\right\} \tag{24}$$

Where $Q = \frac{\kappa}{\rho j}\left[\left(\frac{\partial v}{\partial x} - \frac{\partial u}{\partial y}\right) - 2\phi\right] = \frac{\upsilon_l K}{L_l^2}\left[\left(\frac{\partial v}{\partial x} - \frac{\partial u}{\partial y}\right) - 2\frac{\upsilon_l}{Pr{L_l}^2}\Phi\right]$ is the source term appearing in the equation of micro-rotation.

Concerning the implementation of the boundary conditions, the only unknown distribution function on each wall of the cavity is the one pointing inside the fluid domain. As the values of temperature and micro-rotation are known on the four walls, we use the following relations:

$$\left.\begin{aligned} \theta_{wall} &= \textstyle\sum_{k=0}^4 g_k \\ \Phi_{wall} &= \textstyle\sum_{k=0}^4 h_k \end{aligned}\right\} \tag{25}$$

For instance, if we focus the attention on the left wall, the relations used are:

Global Digital Central
ISSN: 2151-8629

$$\left.\begin{aligned} g_1 &= \theta_{wall} - (g_0 + g_2 + g_3 + g_4) \\ h_1 &= \Phi_{wall} - (h_0 + h_2 + h_3 + h_4) \end{aligned}\right\} \quad (26)$$

4. Heat transfer

The exemplifying plotting of heatlines allows to identify clearly the paths followed by heat flows through the square cavity. More specifically, the heatlines display the microscopic heat transfer process, which is different from the conventional Nusselt number that macroscopically describes the heat transfer rate; they show non-crossed corridors for heat flow and their shapes give a global picture of heat transport. The dimensionless heat function is obtained using a similar procedure as that given in (Raji et *al.*, 2013; Kimura and Bejan, 1983).

The local Nusselt numbers along the horizontal and vertical walls are respectively given by:

$$Nu(X) = -\left(\frac{\partial\theta}{\partial Y}\right)_{Y=0,1} \qquad Nu(Y) = -\left(\frac{\partial\theta}{\partial X}\right)_{X=0,1} \quad (27)$$

Then, the average Nusselt numbers along the horizontal and vertical walls are respectively calculated by the expressions:

$$Nu_{B,T} = \int_0^1 Nu(X)dX \qquad Nu_{L,R} = \int_0^1 Nu(Y)dY \quad (28)$$

The indices B, T, L and R in Eq. (28) stay respectively for bottom, top, left and right walls.

In the oscillatory regime, the mean Nusselt numbers are averaged over one flow cycle as follows:

$$\overline{Nu}_{B,T} = \frac{1}{\tau_p}\int_0^{\tau_p} Nu_{B,T}\, d\tau \qquad \overline{Nu}_{L,R} = \frac{1}{\tau_p}\int_0^{\tau_p} Nu_{L,T}\, d\tau \quad (29)$$

where τ_p stays for a flow period.

5. Numerical validation of the MRT-LBM code

The developed numerical code was first validated against previous works from literature. Table 1 gives a comparison with the benchmark solution of De Vahl Davis (1983) relative to the classical case of a square cavity, differentially heated and filled with air. No significant deviations are observed since the relative differences in terms of Nu, $|\psi|_{max}$, $V_{x,max}$ and $V_{y,max}$ remain within 0.1%, 0.55%, 0.8% and 0.3%, respectively.

Table 1. Numerical code validation in the case of a differentially heated cavity against the bench mark solution of De Vahl Davis (1983).

Ra		10^3	10^4	10^5	10^6	Maximum relative deviation
$Nu_{R,L}$	Our code	1.116	2.240	4.511	8.828	0.1 %
	De Vahl Davis (1983)	1.117	2.238	4.509	8.817	
$\|\psi\|_{max}$	Our code	1.174	5.099	9.662	16.769	0.55 %
	De Vahl Davis (1983)	1.174	5.071	9.612	16.750	
U_{max}	Our code	3.649	16.267	35.008	64.624	0.8 %
	De Vahl Davis (1983)	3.649	16.178	34.73	64.63	
V_{max}	Our code	3.699	19.688	68.603	219.667	0.3 %
	De Vahl Davis (1983)	3.697	19.617	68.59	219.36	

The validity of the computer code has been also checked by comparing our results against those obtained by Aydin and Pop (2007) for the problem of natural convection in a square cavity differentially heated and filled with a micropolar fluid (formulation taking into account the effect of the presence of micoparticle structures in the working fluid). We have reproduced the results obtained by these authors using a mesoscopic approach (LBM code) recently developed in our laboratory. Comparative results obtained with $Ra = 10^6$ are presented in Fig. 3 in terms of streamlines and isotherms for $K = 1$ and 2. The qualitative comparison shows an excellent agreement between the results presented. In addition, the quantitative comparisons in terms of Nu show also excellent agreements with maximum differences of about 0.86% from the results published by Aydin and Pop (2007).

Table 2 Grid effect in terms of Nu_{max} and period τ_p for $Ra = 10^6$ and $K = 2$.

Grid	Nu_{max}	τ_p
80×80	5.903	0.0176
120×120	5.899	0.0175
160×160	5.899	0.0175

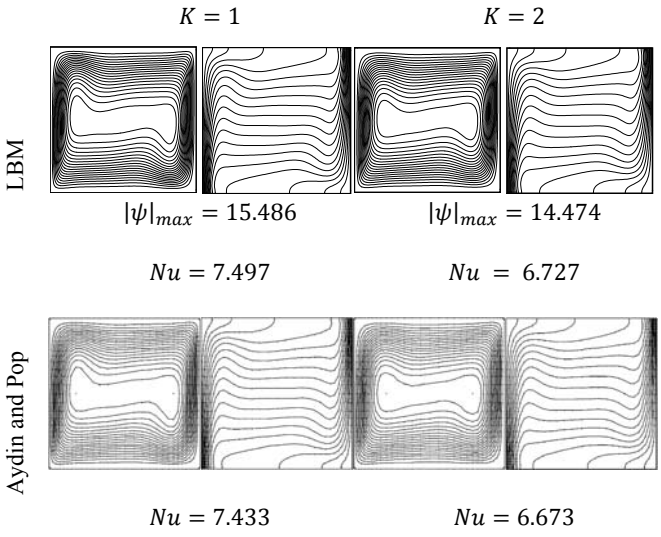

Fig. 3 Validation of the MRT-LBM code against classical methods in the case of a micropolar fluid for $Ra = 10^6$.

All the results presented in this study were obtained with a grid of 120×120. The choice of this grid was based on preliminary tests evaluating the sensitivity of the results vis-à-vis of the grid change. Numerous tests conducted in the unsteady regime with $Ra = 10^6$ (results not presented) have shown that the selected grid is enough to describe in a satisfactory manner the fluid flow and heat transfer characteristics. We simply illustrate here the effect of the grid for a selected case in the oscillatory regime. This effect on the oscillation period τ_p and maximum value of the average Nusselt number is examined for $Ra = 10^6$ and $K = 2$ (oscillatory case). Table 2 shows clearly the insensitivity of the results to the mesh refining when the latter is changed from 120×120 to 160×160.

6. Results and discussion

Natural convection in a square cavity heated from below, cooled from above and submitted to a linearly varying temperature from its vertical sidewalls is studied numerically using the lattice Boltzmann method. The

Global Digital Central
ISSN: 2151-8629

Rayleigh number, Ra was from 10^3 and 10^6 and the vortex viscosity parameter, K, which reflects the behavior of the micro-particles existing in the basic fluid was from 0 (a Newtonian case) to 2 (micropolar fluid). The preliminary tests conducted have shown that, dependently on the governing parameters, the final state of the flow could be either steady or unsteady. In addition, the present problem is characterized by a multiplicity of solutions and each solution has its own range of existence in the steady regime depending on the nature of the fluid. The behavior of the latter vis-à-vis of the imposed boundary conditions is discussed in the following subsection, first for the Newtonian case and then for the micropolar fluid.

6.1. Newtonian case: steady and oscillatory regimes

For this problem, three different steady solutions have been obtained despite the demarcation from the pure Rayleigh-Bénard problem by imposing linear profiles to the temperature on the vertical boundaries of the cavity. Figs. 4 illustrate these solutions for $Ra = 3 \times 10^4$; value within the common existing range of the three solutions. Fig. 4a, exemplifying the first kind of solution, shows a structure constituted by a monocellular diagonal dominant flow (MDF) and two recirculating positive cells located in two opposite corners, those connected by the second diagonal of the cavity. The dominant negative cell is clockwise rotating and almost 15.5 times more intense than the small positive recirculating cells. The MDF appears with the birth of convection and persists by increasing Ra up to $\mathrm{Ra} = 3.9 \times 10^4$. The image of this solution from a vertical mirror is also a solution of the problem constituted by a positive dominating cell and two recirculating negative vortices. Both solutions, the MDF and its mirror image, lead to identical average Nusselt numbers. In addition, each solution is symmetrical with respect to the center of the cavity as it can be seen in the streamlines and the corresponding isotherms. The latter show important gradients, mainly in the central regions of the horizontal walls and the temperature distribution is obviously affected by the form of the negative dominant cell and its clockwise rotation. The heatlines paths give a more indicative idea on how the heat is transferred by the working fluid from the heated surfaces to the colder ones. Thus, the inspection of the heatlines of Fig. 4a shows that, due to the clockwise rotation of the main cell, the heat is supplied to the fluid by the right vertical wall (contact between the cooled cell's lines and this wall) and the horizontal bottom one. The evacuation of heat occurs through the left vertical wall (contact between the heated cell and this wall) and mainly through the top horizontal one. In addition, the examination of the heatlines shows closed lines inclined similarly to the streamlines, indicating the existence of a thermally inactive area. The heat exchange between the active walls occurs outside this area as indicated in the figure. Note that for the mirror solution, the main rotation is counter-clockwise and the vertical walls change the role (the left/right one supplies/evacuates heat). Furthermore, the rate of heat exchange (in mean values) between the fluid and two parallel walls is equivalent (more details on this fact are evoked later).

The second type of solution, presented in Fig. 4b, is a bicellular vertical ascending flow (BVAF) with two very small vortices (not visible in the figure) located near the left and right lower corners of the cavity ($|\psi_{ext}| = 0.0321$). This solution, obtained in the range $1.6 \times 10^4 \leq Ra \leq 5.7 \times 10^4$, is symmetrical with respect to the vertical centerline of the cavity. In fact, under the effect of the lower heating horizontal wall, the fluid is conveyed upward in the central part of the cavity. Each of both flow cells is cooled on the upper part of the fluid domain while its peripheral lines move along the cold horizontal wall, towards a vertical surface. The most important heat exchange between the heated fluid and the cold wall occurs, as expected, in the central part of the cold surface; there where the ascending jet of the heated fluid interacts with this surface. Broadening the knowledge concerning the heat transfer process for the BVAF, requires the examination of heatlines of Fig. 4b where we note the existence of two zones of inactive areas (closed lines) from either side of the vertical centerline of the cavity. The closed heatlines show some similarity with the flow cells due to the non-negligible effect of convection. The examination of the open lines indicating the path of the heatlines ensuring the thermal interaction between the active walls, points out that heat provided to the fluid by the vertical walls and, predominantly, by the lower horizontal surface, is transported upward by the ascending current of the bicellular flow, between the inactive areas. For this structure, the heat is mainly evacuated through the upper cold wall and the vertical walls, which preheat the fluid before it interacts with the former (the lower heated surface), hamper the contribution of the lower surface.

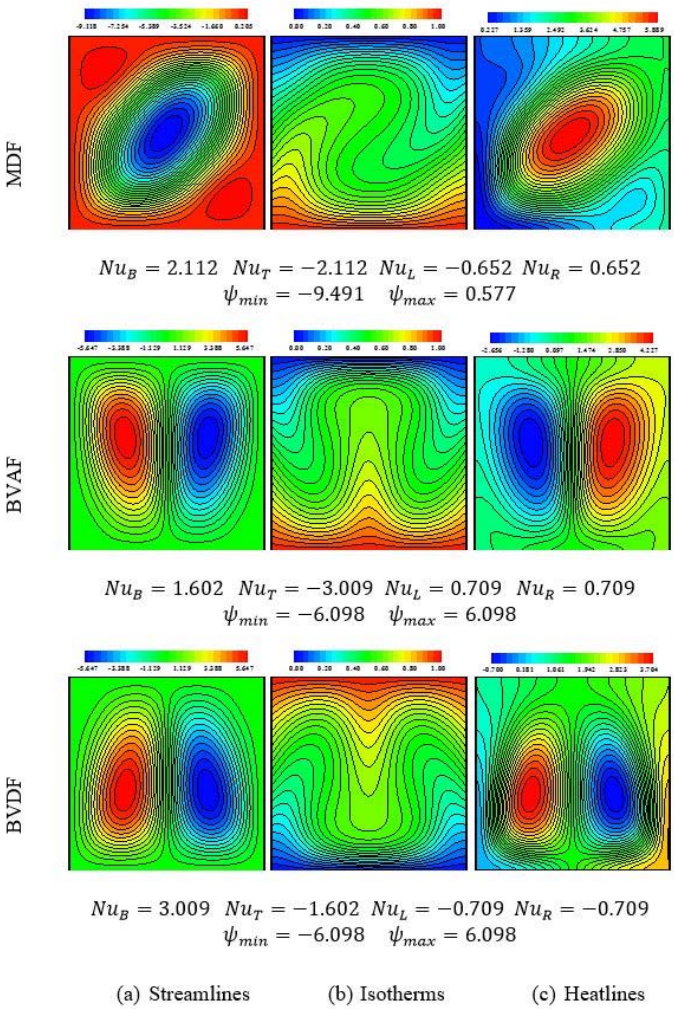

Fig. 4 Streamlines (a), isotherms (b) and heatlines (c) corresponding to stationary solutions obtained with Ra = 3×104.

Fig. 4c illustrates the third kind of steady solution obtained in this study which is a bicellular vertical descending flow termed BVDF. Both cells constituting the BVDF are ascending/descending along the vertical sides/centerline of the cavity since the left/right cell is clockwise/counter-clockwise rotating. Evidently, the dominating cells are of equal intensity because of the symmetry of the BVDF solution. Despite this bicellular dominating nature of the flow, two small vortices (not visible in the streamlines) with very weak intensities ($|\psi| = 0.0322$) are however existing, their locations are observed near the left and right upper corners of the cavity. It is to note that the intensities of the main cells and the secondary ones are curiously identical to those of Fig. 4b. In the meantime, the streamlines and isotherms of Fig. 4c are perceived as images of the corresponding streamlines and isotherms of Fig. 4b through a horizontal mirror. The important gradients of temperature are observed in the central part of the lower heated wall, there where the descending

Global Digital Central
ISSN: 2151-8629

cooled streams of the BVDF meet this wall. The heatlines corresponding to this solution show a different process of heat transfer. In fact, all the open lines ensuring the transport of heat leave the lower hot wall. A part of the transported heat is evacuated from the vertical walls and the remaining part (the most important) through the cold wall. The paths followed by the open lines and the structure of the closed heatlines (thermally inactive zones) of the BVDF cannot be deduced as images through a mirror from those of the BVAD. For the BVDF structure, the lower heated wall mainly provides the heat and the contribution of the upper surface to the evacuation of heat is reduced by the contribution of the vertical walls in the evacuation process. The existence ranges of the BVDF and BVAF are identical and, for both solutions, weak periodic oscillations were observed just above the upper limit of their common existence range, marking the onset of the oscillatory periodic regime. This behavior results from the progressive amplification of the secondary cells, supported by the increase of Ra, which end up competing with the main cells in favor of the appearance of the oscillatory regime (OR). The latter occurs at the threshold value $Ra_B = 5.7 \times 10^4$. Above this critical value, the flow oscillates between monocellular diagonal flows, passing through intermediate states showing complex structures during the evolution of the flow cycle. It should be specified that the three steady solutions described before coexist in the range $1.6 \times 10^4 \leq Ra \leq 3.9 \times 10^4$. Within this common range, the convergence of the numerical code towards one of these three solutions depends on the initial conditions used to start the calculations. It is also useful to outline that the threshold Ra_B of Rayleigh number from which the transition towards the OR occurs is obtained by progressively increasing Ra and using the steady bicellular flow as initial condition. However, the threshold towards the oscillatory regime occurs prematurely (at $Ra_M = 5 \times 10^4$) if the steady MDF is used to start the calculations. Moreover, by varying Ra in the range $3.9 \times 10^4 < Ra < 5 \times 10^4$, the use of the MDF and its mirror image as initial condition leads to the obtaining of both types of the bicellular flow (transitions illustrated later in Fig. 14).

The oscillatory regime is illustrated in Fig. 5a in terms of ψ_{max} and ψ_{min} and in Fig. 5b in terms of instantaneous mean Nusselt numbers on four walls of the cavity. Fig. 5a shows that the variations of ψ_{ext} vs. time are characterized by periodic oscillations with very important amplifications during the evolution of the cycle. The peaks observed in the evolutions of ψ_{max} and ψ_{min}, show that the diagonal flow (either clockwise or counter-clockwise) dominates completely during short intervals of time while the secondary cells' intensities become minimal within these intervals. These secondary cells are in fact at the origin of the oscillatory flow (as mentioned before) and their signs are opposite to those of the dominant one. The oscillations of the mean Nusselt numbers on four walls of the cavity are also of periodic nature as it can be seen in Fig. 5b and their signs depend on either if heat is received (positive sign) or lost (negative sign) by the fluid through the boundaries of the cavity. In the oscillatory regime, the streamlines exemplified in Figs. 6 at the selected instants P1, P2, …, P6 in Fig. 5a indicate that the flow oscillates between two extreme states each of them characterized by the dominance of a diagonal cell either negative (instant corresponding to P1) or positive (instant corresponding to P3). Thus, each of the main diagonal cells dominates for a moment during one-half of the cycle. For instance, the instant corresponding to P1 in Fig. 6 illustrates the domination of the diagonal negative cell. After this moment, the dominant cell weakens in favor of the secondary positive ones and finishes by breaking up (the instant corresponding to P2 in Fig. 5a shows almost the breaking threshold of the negative cell) under the effect of the latter (the positive ones). This evolution leads to the birth of a complex multicellular structure constituted by four cells at a certain moment of the cycle, followed by the merging of the initially secondary cells to form a new diagonal positive dominating cell. In the second half of the flow cycle, the diagonal positive cell and the secondary negative ones play similar roles to those of the diagonal negative cell and the positive secondary ones in the first half of the cycle, respectively. The examination of the oscillations' nature accompanying the increase of Ra in the oscillatory regime showed that the results obtained with $Ra = 9 \times 10^5$ are still monoperiodic. However, at $Ra = 10^6$, the solution is characterized by oscillations of biperiodic nature (results not illustrated here) and the latter are maintained until the appearance of the chaotic regime. This indicates that the passage from monoperiodic to biperiodic oscillations occurs for a threshold value within the short interval $]9 \times 10^5, 10^6]$. Finally, within each flow cycle, each figure of streamlines and isotherms at a given instant have its mirror image in the same cycle. In addition, since the instantaneous streamlines and isotherms and their images lead to same instantaneous mean Nusselt numbers in absolute value, it follows that one flow period is twice that of the instantaneous average Nusselt numbers. More details can be deduced by observing the temporal evolutions vs. time of ψ_{ext} and average Nusselt numbers depicted respectively in Figs. 5a and 5b. For instance, the maximum values of Nu on top and bottom walls are reached for the quadra-cellular flow structure which ensures a good contact of surface between the peripheral lines and the neighboring horizontal surfaces. Moreover, for the same cycle instant, Nu on the left and right walls is nil due to the local Nusselt number symmetry with respect to the central point of vertical walls ($Y = 0.5$).

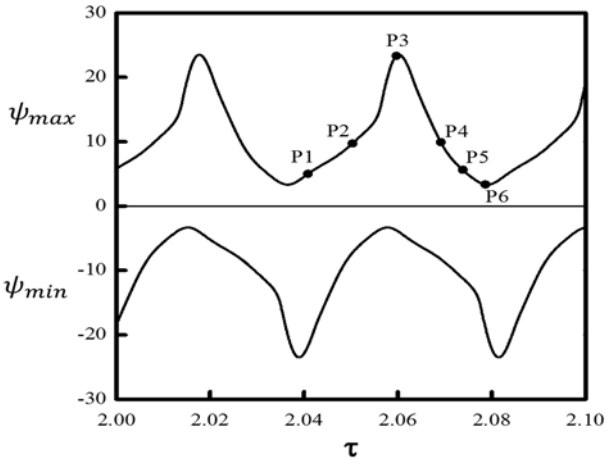

(a)

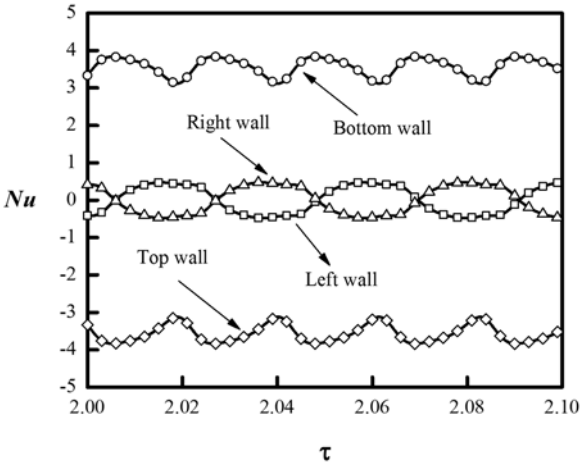

(b)

Fig. 5 Temporal variations of ψ_{ext} (a) and Nu (on the active walls) (b) for $Ra = 10^5$.

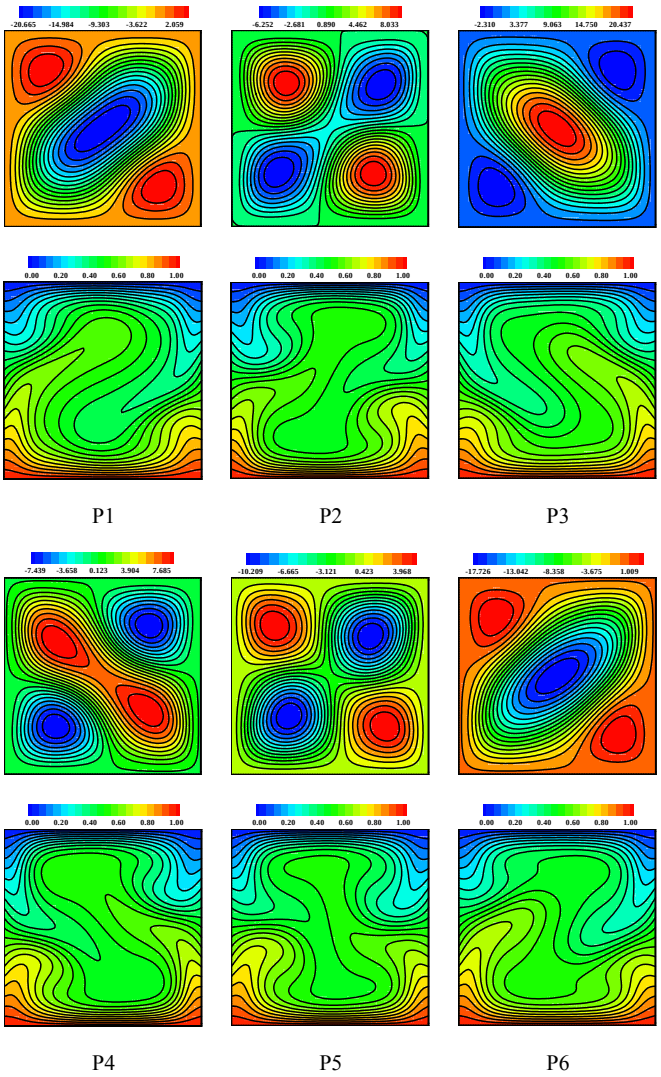

Fig. 6 Streamlines and isotherms at selected instants in Fig. 5a for Ra $=10^5$.

Table 3 Delimitation of the existence ranges of solutions in terms of $Ra\times10^{-4}$ and various K.

K		0		1		2	
Numerical method		FDM	LBM	FDM	LBM	FDM	LBM
MDF	From	0.5	0.5	1	1.1	1.6	1.6
	To	3.7	3.9	7.5	7.6	11	11
BVAF	From	1.7	1.6	3.3	3.5	5	5
	To	5.5	5.7	11	11	18	18
BVDF	From	1.7	1.6	3.3	3.5	5	5
	To	5.5	5.7	11	11	18	18
OR	From	4.9	5	9.8	9.8	15	15
	To			100			

6.2. Micropolar case: steady and oscillatory regime

In table 3, we specify the existence range of each type of the four solutions (three steady-state solutions and an oscillatory one) obtained with both LBM and FDM. The FDM results are also presented in this table for a complementary objective of validation. We can notice that the parameter K plays an important stabilizing role, which consists in delaying both the onset of convection and the transition from the steady-state regime to the oscillatory one (Hopf's bifurcation). This delay, engendered by the non-Newtonian behavior, shifts the common existence range of the steady solutions and the onset of the oscillatory regime towards higher Rayleigh numbers. The important delay recorded in the transition to the oscillatory regime makes the existence range of the steady solutions increasingly wider by increasing the parameter K(3 times wider by increasing K from 0 to 2).

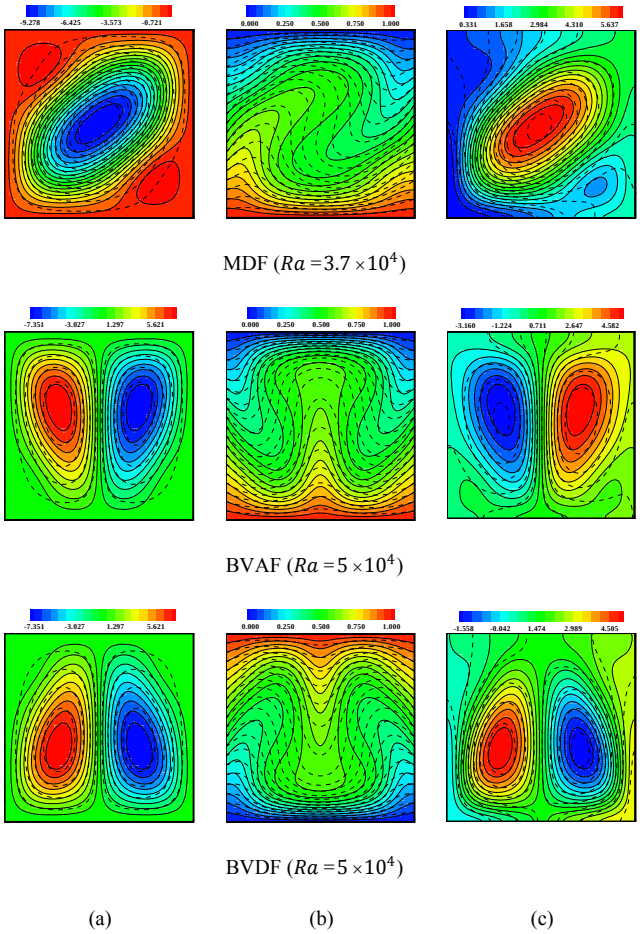

Fig. 7 Streamlines (a), isotherms (b) and heatlines (c) for $K = 0$ (solid lines) and $K = 1$ (dashed lines).

For a close inspection of the effect engendered by the non-Newtonian behavior of the micropolar fluid, we exemplify in Fig. 7 comparative streamlines, isotherms and heatlines for $K = 0$ (Newtonian case) and $K = 1$ (micropolar fluid). We can observe that the increase of K engenders a decrease of the small vortices' size leading to more stable flows with smaller intensities compared to the Newtonian case. For instance, the intensities of the small vortices drop from $|\psi_{ext}| = 0.992$ to $|\psi_{ext}| = 0.153$ for the MDF solution and from $|\psi_{ext}| = 0.348$ to $|\psi_{ext}| = 0.010$ for the bicellular case (both BVDF and BVAF). This indicates clearly that the reinforcement of these small cells requires higher Ra in the case of the micropolar fluid to reach the critical size and intensity causing the transition towards the oscillatory regime. Indeed,

Global Digital Central
ISSN: 2151-8629

the retard observed in the transition towards the oscillatory regime for the non-Newtonian fluid is explained by the increase of the viscous forces accompanying the increase of K, which slows down the fluid circulation according to the damping role of viscosity. The effect of the viscosity increase, associated to the increase of K, is well visible on the isotherms; the latter are less tight near the active walls indicating a perceptible deterioration of the thermal interaction between the active walls and the working fluid. In addition, the increase of the viscosity effect leads to an attenuation of the isotherms' distortion, particularly in the central area of the cavity. The examination of the heatlines presented in Fig. 7 shows a perceptible demarcation between the dashed ($K = 1$) and full ($K = 0$) lines for both closed heatlines of the inactive area and the open lines indicating the paths borrowed by heat from the warmer surfaces to the colder ones. Generally, it can also be retained that the trends remain similar by increasing K from 0 to 1 with a noticeable shifting of the open lines toward the center of the upper wall.

More details relative to the impact of the viscosity increase (increase of the parameter K) are perceived in Fig. 8 exemplifying the vertical component of velocity profiles at mid-height of the cavity ($Y = 0.5$), along the horizontal direction. In Fig. 8, the damping role of the parameter K is well confirmed in the velocity profiles, which show important reductions in absolute values of the extremums of velocity. The most important reductions, engendered by the increase of K, are observed in the central part of the cavity for the ascending (case of BVAF) and descending (case of BVDF) flows of the bicellular structures. Quantitatively, the maximum attenuations reached for velocity are about 58.05% for the bicellular flows (in the central part of the cavity) and about 44.90% for the monocellular diagonal flow (approximately midway between each vertical wall and the center of the cavity) when the parameter K is increased from 0 to 2.

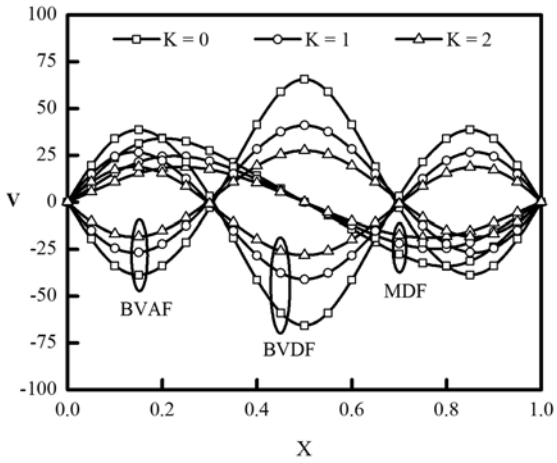

Fig. 8 Mid-height (Y = 0.5) velocity profiles along the horizontal mid-plane obtained for the MDF at Ra=3.7×10^4 and BVAF and BVDF at Ra=5×10^4.

In the unsteady regime, we illustrate the temporal variations of ψ_{max} and ψ_{min} (Fig. 9a) and the instantaneous average Nusselt numbers on the active walls of the cavity (Fig. 9b) for $Ra = 5 \times 10^5$ and various values of K. Recall that, in the unsteady periodic regime, the mean values of the Nusselt numbers on the vertical/(horizontal) walls are identical in absolute values. These figures demonstrate that the increase of the parameter K does not alter the periodic nature of the solution. However, it leads to a noticeable reduction of the amplitudes of oscillation (the reduction alters rather the maximum in absolute values of ψ_{ext}) and a rise of their periods because of the flow slowness, which leads to longer flow cycles. In the case of heat transfer, Fig. 9b indicates that the increase of K affects both the maximum and the minimum of the instantaneous average Nusselt numbers on the horizontal walls. For instance, for $K = 1/(2)$, the maximum of Nu_B is close /(lower) to/(than) the minimum of $K = 0$. Despite the fact that the increase of K engenders an increase of the amplitude and the period of oscillations for Nu_B, the latter (the oscillations) fluctuate around mean values much lower than those corresponding to the Newtonian case ($K = 0$). The contribution of the vertical walls to the heat exchange are evaluated through Nu_L and Nu_R. The increase of K leads to a change in the amplitude and oscillations' period of these quantities but the averaged values of the latters over flow cycles remain insensitive to the increase of K ($\overline{Nu}_R = \overline{Nu}_L = 0$). Note finally that, the instantaneous flow structures obtained with the micropolar fluid show big similarities with those of Fig. 6 corresponding to $K = 0$ in the oscillatory regime. Each flow cycle corresponding to $K \neq 0$, admits a corresponding similar cycle with $K = 0$ but reached with some delay due to the important viscous effects of the micropolar fluid.

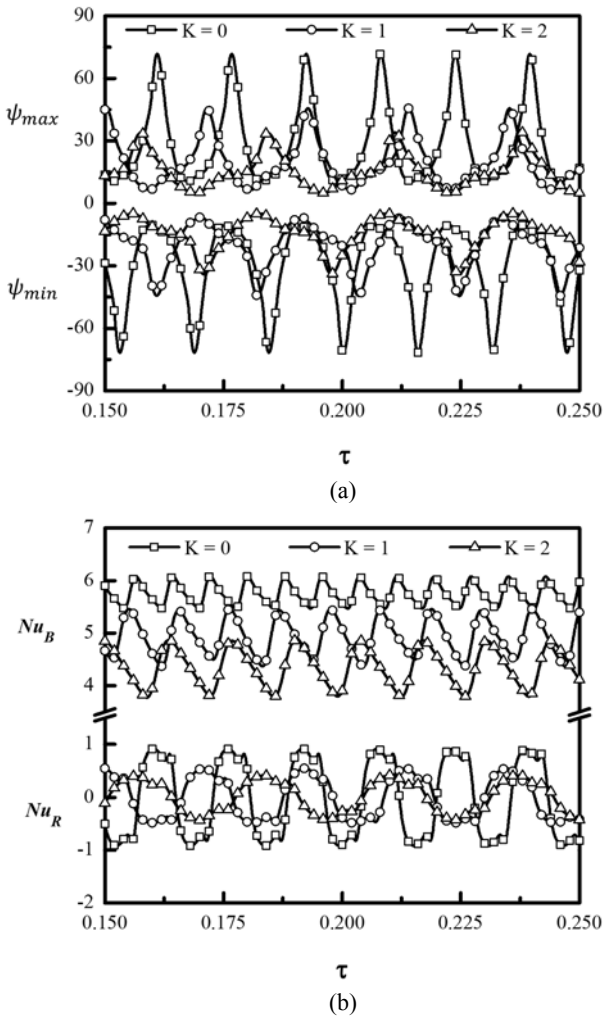

Fig. 9 Temporal variations of ψ_{ext} (a) and $Nu_B(= -Nu_T)$ and $Nu_R(= -Nu_L)$ (b) for $Ra = 5 \times 10^5$.

7. Heat transfer

7.1 Local heat transfer on active walls

For the case of the Newtonian fluid, Fig. 10 exemplifies the local Nusselt numbers profiles along the vertical ($Nu_L(Y)$ and $Nu_R(Y)$) and horizontal ($Nu_B(X)$ and $Nu_T(X)$) walls for two values of Ra. These values of Ra are selected in the common existence range of the three steady solutions

and correspond to the lowest and highest values of Ra delimiting this common range which are $Ra = 1.6 \times 10^4$ (filled circles) and $Ra = 3.9 \times 10^4$ (empty circles), respectively. For the MDF, Fig. 10a shows that, despite the same linear profile imposed to the vertical walls, the sign of the local Nusselt numbers $Nu_R(Y)$ and $Nu_L(Y)$ are opposite ($Nu_R(Y) > 0$) and ($Nu_L(Y) < 0$). This means that the right/left vertical wall provides/evacuates heat to/from the working fluid. These signs are imposed by the nature of the clockwise rotating flow (the dominant cell) of Fig. 4a and are expected to change for the solution image through a vertical mirror. For the remaining walls, which are submitted to imposed heating (lower horizontal wall) and cooling (upper horizontal wall) with constant temperatures, the fluid receives heat from the lower horizontal wall and releases it through the upper horizontal one either for the presented solution or its image. Note that the curves of the local Nusselt numbers of any two opposite walls display a symmetry with respect to the center of the cavity. In addition, the quantitative differences engendered by the augmentation of Ra are perceptible in some locations (there where the interaction fluid-wall is important) and negligible in others (there where the interaction fluid-wall is of less importance).

Regarding the examination of Figs. 10b and 10c, exemplifying local Nusselt numbers profiles on the active walls respectively in the case of the BVAF and BVDF, it is seen that $Nu_L(Y)$ and $Nu_R(Y)$ curves are perfectly coincident for both types of solutions due to the symmetry of the latter. For the bicellular flow, the vertical walls contribute at the same time and in the same way to the fluid heating (case of the BVAF) or cooling (case of the BVDF). In addition, the negative/positive sign of $Nu_L(Y)$ and $Nu_R(Y)$ in the case of the BVAF/BVDF indicates that the cooled/heated fluid moving downward/upward along the vertical walls continues to receive/release heat from/to these boundaries throughout much of their lengths. The relatively weak values of $Nu_L(Y)$ and $Nu_R(Y)$ show that the modest contribution of the vertical boundaries in terms of heat amounts received or liberated by the fluid through these boundaries. On the horizontal walls, $Nu_B(X)$ and $Nu_T(X)$ keep-unchanged signs which are respectively positive and negative due to the key role played by the lower/upper surface in the heating/cooling process. Note that the profiles of $Nu_B(X)$/ $Nu_T(X)$ of the BVAF can be deduced (and vice-versa) from those of $Nu_T(X)$/ $Nu_B(X)$ of the BVDF by using the simple symmetry rule with respect to the center of the cavity. Similarly, the profile of $Nu_L(Y)$ (or $Nu_R(Y)$) corresponding to each of the bicellular flow can be deduced from $Nu_L(Y)$ (or $Nu_R(Y)$) of the other bicellular flow by using the centro-symmetry allowed in the case of these solutions. It is also interesting to note that the increase of Ra leads to an important local increase of $Nu_B(X)$ and $Nu_T(X)$ with maximum amplifications in the central region (case of $Nu_B(X)$/ $Nu_T(X)$ of the BVDF/BVAF) or between the center of the wall and one of its extremities (case of $Nu_T(X)$/ $Nu_B(X)$ of the BVDF/BVAF). For the vertical walls, the quantitative impact of the Rayleigh number increase on $Nu_L(Y)$ and $Nu_R(Y)$ is visibly limited, displaying a maximum local improvement of about 39%. It is interesting to outline that the plot (results not presented here) of the local Nusselt numbers of the micropolar fluid, obtained with $K = 2$, for the limiting Ra values ($Ra = 3.5 \times 10^4$ and 7.6×10^4) of the common existence range of the three solutions has caught our attention by a surprising behavior. In fact, for $K = 2$, the local Nusselt profiles corresponding to $Ra = 3.5 \times 10^4/7.6 \times 10^4$ were found identical to their corresponding profiles of the Newtonian case ($K = 0$) and obtained with $Ra = 1.6 \times 10^4/3.9 \times 10^4$. This means that, probably, the steady results of the non-Newtonian case can be deduced from those of the Newtonian results with some delay in terms of critical Ra (which depends on K). The comparative results presented in Fig. 11 support this deduction since the maximum and minimum relative differences observed in the limits of the common ranges of the three solutions, and in the limits of the existence range of each solution for K = 0, 1 and 2 remain within 8.28% and 1.26%, respectively. The difference is probably attributed to the approximate determination of the Ra values delimiting the common existence range of the different solutions and those leading to the unsteady regime for the three considered values of K.

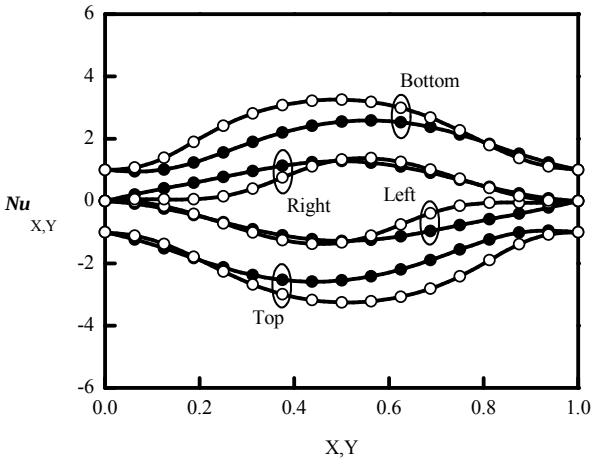

(a)

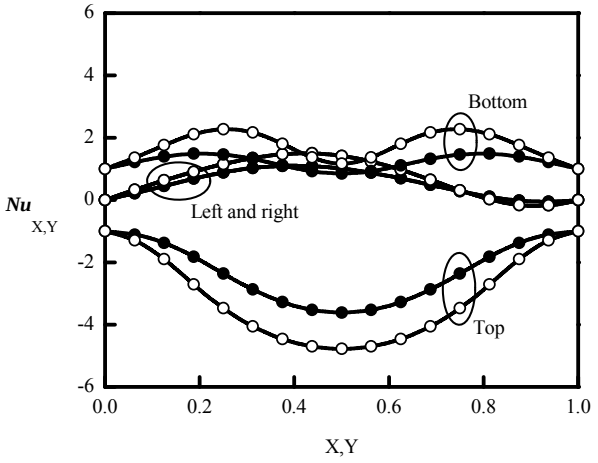

(b)

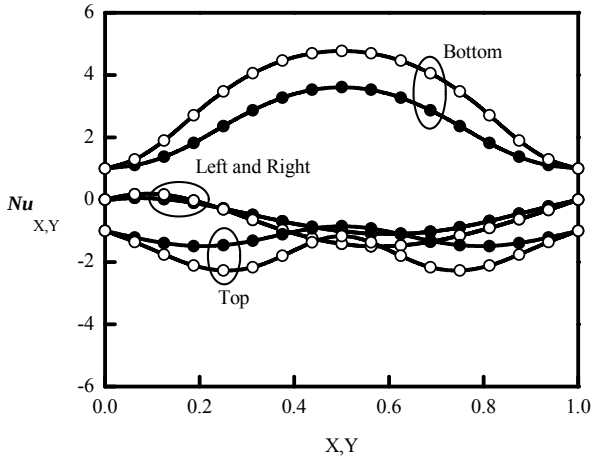

(c)

Fig. 10 Local Nusselt numbers obtained at the extreme limits of the common existence range for $K = 0$ (●Ra=1.6×10^4 ○Ra=3.9×10^4): (a) MDF, (b) BVAF and (c) BVDF.

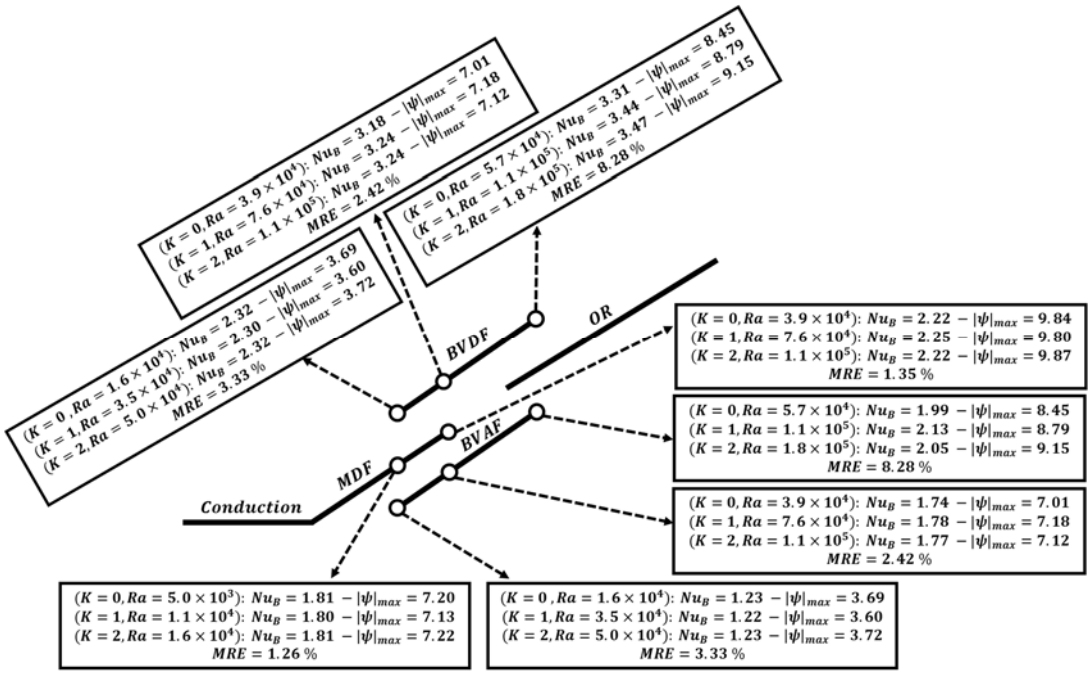

Fig. 11 Comparisons of Nu_B and $|\psi|_{max}$ in the extreme limits of the common existence ranges of the three steady solutions and those from which transitions to oscillatory regime occur.

7.2 Average heat transfer

The mean Nusselt values on the vertical walls submitted to linear variations of temperature are identical, and those evaluated on the horizontal surfaces are identical in the case of steady MDF and unsteady regime. For the bicellular flows, it is found that $|Nu_B|/|Nu_T|$ is larger than $|Nu_T|/|Nu_B|$ in the case BVDF/BVAF although they have the same intensities. This is due to the path followed by the fluid leaving the bottom wall. The latter moves up towards the top cold wall through the central region of the cavity in the case of the BVAF, while it moves up along the vertical walls (where it loses a part of its heating capacity) in the case of the BVDF. In Fig. 12, we illustrate only the variations, versus Ra, of the average Nusselt number on the bottom wall to indicate the different transitions observed in this study. Further results relative to the mean Nusselt numbers on all active walls are given in Table 4. In this figure both steady ($Nu_{B,L}$) and unsteady ($\overline{Nu}_{B,L}$) regimes are presented for two values of K illustrating the Newtonian ($K = 0$) and non-Newtonian (K = 2) behaviors. The arrows in this figure indicate the transition type undergone for each solution while progressively varying Ra. Red and blue arrows indicate the directions of the transitions observed respectively by increasing and decreasing Ra. A close inspection of Fig. 1**2** shows that the transition from the conductive regime to the convective one occurs at $Ra \approx 5 \times 10^3$ with the birth of the monocellular diagonal dominating flow (the only solution obtained for lower values of Ra in the presence of convection). For $K = 2$, the transition from the conductive regime occurs towards the same type of flow (monocellular diagonal flow) and it is considerably delayed (it occurs at $Ra \approx 1.6 \times 10^4$) for the micropolar fluid due to the more important viscous effects. The two secondary cells, located in opposite corners and aligned on the second diagonal of the cavity are behind the instability of the MDF. In fact, for this type of flow, the increase of Ra supports the secondary cells up to a certain limit from which the centro-symmetry of the flow is destroyed to ensure the transition towards the BVAF (at $Ra = 3.9 \times 10^4$) characterized by a symmetry with respect to the vertical centerline of the cavity. This transition is accompanied by a noticeable deterioration (results of the MDF being the reference) in terms of heat exchange between the lower heated wall and the neighboring fluid. By using a solution of the BVAF as initial condition and increasing/(decreasing) progressively Ra, we assist to a new transition towards the (OR)/(MDF) at $5 \times 10^4/(1.6 \times 10^4)$. Both transitions of the BVAF towards the MDF/(OR) obtained by decreasing/(increasing) Ra are accompanied by an increase of the mean Nusselt number. For the other type of bicellular flow, namely the BVDF, it was obtained with the considered mesh from the image of the MDF through a vertical mirror by increasing Ra until it exceeds the threshold 3.9×10^4. Moreover, the BVDF was also obtained by decreasing Ra in the unsteady regime to its lower limit. Just below this limit, the steady regime is recovered, and the numerical code converges either towards the BVDF or the BVAF depending on the initial conditions (i.e. the flow structure at the moment ending the calculations in the unsteady regime). In the steady regime, the BVDF is the most favorable to the interaction between the heated bottom wall and the centrally descending fluid.

Table 4 provides useful indications, relative to the global contributions of the active walls to the heating (positive values) and/or cooling (negative values) processes. The inspection of this table indicates that the vertical boundaries play different roles depending on the type of solution. Globally, the results presented in this table show that the fluid receives heat from its right vertical wall ($Nu_R > 0$) and loses an equivalent amount of heat through the left vertical boundary ($Nu_L = -Nu_R < 0$) in the case of the MDF. For this type of flow, we notice also that $Nu_B = -Nu_T > 0$, demonstrating that an equivalent amount of heat supplied by the lower wall to fluid is evacuated through the upper cold surface. The situation is different for the bicellular flow since, at the same time, both vertical walls play a heating role (case of the BVAF for which $Nu_L = Nu_R > 0$) or a cooling role (case of the BVDF for which $Nu_L = Nu_R < 0$) in the process of heat exchange between the working fluid and these boundaries. Note that the positive/negative contribution of the vertical walls to the heat exchange in the case of the BVAF/BVDF occurs to the detriment of the bottom/top surface, which provides/evacuates less heat to/from the working fluid. The results presented in table 4 show also

Global Digital Central
ISSN: 2151-8629

that, for each type of solution, the thermal contribution of the four active walls is deteriorated (deterioration more important in terms of proportion for the horizontal walls) for the case of micropolar fluid in comparison with the Newtonian case. Note finally that, as indicated in table 4, the mean contribution in terms of heat exchange of the vertical walls is null ($\overline{Nu}_L = \overline{Nu}_R = 0$) over a flow cycle of the unsteady periodic regime.

Table 4 Mean Nusselt numbers on the active walls of the cavity and extremum values of ψ at selected values of Ra.

		Nu_B or $\overline{Nu}_B$	Nu_T or $\overline{Nu}_T$	Nu_L or $\overline{Nu}_L$	Nu_R or $\overline{Nu}_R$	ψ_{min} or $\bar{\psi}_{min}$	ψ_{max} or $\bar{\psi}_{max}$
$K = 0$	MDF $Ra = 3\times10^4$	2.112	-2.112	-0.652	0.652	-9.491	0.577
	BVAF $Ra = 3\times10^4$	1.602	-3.009	0.709	0.709	-6.098	6.098
	BVDF $Ra = 3\times10^4$	3.009	-1.602	-0.709	-0.709	-6.098	6.098
	OR $Ra = 5\times10^5$	5.753	-5.753	0	0	29.168	-29.164
$K = 1$	MDF $Ra = 5\times10^4$	2.0355	-2.0355	-0.688	0.688	0.388	-8.917
	BVAF $Ra = 5\times10^4$	1.494	-2.845	0.680	0.680	5.359	-5.359
	BVDF $Ra = 5\times10^4$	2.845	-1.494	-0.680	-0.680	5.359	-5.359
	OR $Ra = 5\times10^5$	4.933	-4.933	0	0	19.684	-19.885
$K = 2$	MDF $Ra = 10^5$	2.201	-2.201	0.597	0.597	0.795	-9.821
	BVAF $Ra = 10^5$	1.710	-3.160	0.731	0.731	6.685	-6.685
	BVDF $Ra = 10^5$	3.160	-1.709	-0.731	-0.731	6.685	-6.685
	OR $Ra = 5\times10^5$	4.292	-4.291	0	0	15.001	15

Thus, for all periodic unsteady results presented in this study, $\overline{Nu}_B = -\overline{Nu}_T$, demonstrating that, over each flow cycle, the mean quantity of heat provided to the fluid by the lower wall is equivalent to that evacuated through the upper cold surface of the cavity. These results show that the extraction of heat from the hot wall (the cooling process of the lower hot wall) depends strongly on the type of solution induced (i.e. initial perturbation). At $Ra = 3\times10^4$ and $K = 0$, for example, the best/worst cooling is performed via the BVDF/BVAF. In fact, the amount of heat extracted from the bottom hot wall in the case of the BVDF is nearly twice that of the BVAF although these two solutions are simply mirror images of each other. The rate of cooling ensured by the MDF is about 2/3 of that corresponding to the BVDF. Thus, if the objective is to minimize the heat losses from the bottom wall, the BVAF is the appropriate solution.

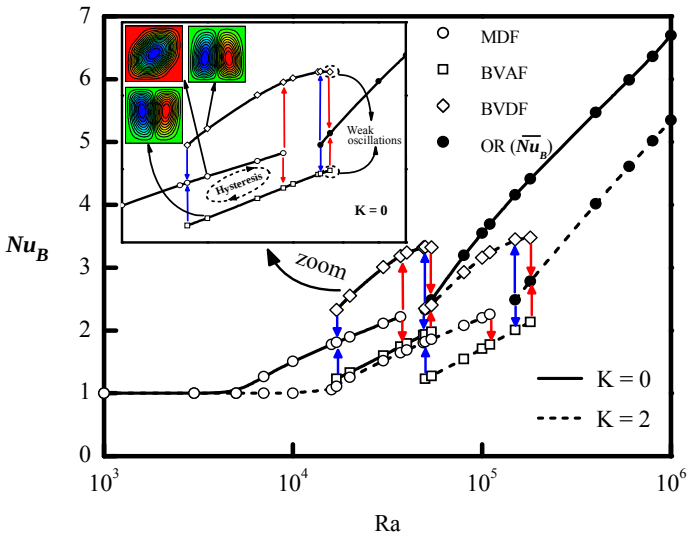

Fig. 12 Average Nusselt number on the bottom wall variations versus Ra for $\boldsymbol{K} = \mathbf{0}$ and **2**.

8. CONCLUSIONS

A numerical study of natural convection involving a micropolar fluid confined in a Rayleigh-Bénard square cavity submitted in addition to linearly variable temperatures along the vertical sides is conducted using the Lattice-Boltzmann method. The collision process of the latter is performed by the multi-relaxation time scheme. Qualitative comparisons between Newtonian and micropolar fluids are presented in terms of streamlines, isotherms, heatlines and velocity and local Nusselt numbers profiles. Quantitative comparisons have been illustrated in terms of Nusselt numbers. The multiplicity of steady solutions (up to three solutions have been obtained) is demonstrated and the MRT-LBM was experimented successfully in predicting the existence range of each solution and the thresholds leading to the unsteady regime. The damping role of the micropolar fluid, characterized by the delay of transitions (increase of the critical Rayleigh numbers) and the slowdown of the flow circulation is confirmed. The results presented show that the BVAF and the BVDF promote respectively the heat evacuation through the top cold surface and the heat extraction from the bottom hot wall. This means that, depending on the objective, this configuration could be used either to ensure an efficient cooling of the bottom hot wall by promoting the BVDF or to minimize heat losses from the latter wall by promoting the BVAF. The amount of heat extracted by the BVDF from the bottom wall is about twice that extracted by the BVAF.

REFERENCES

Aounallah, M., Belkadi, M., Adjlout L. and Imine, O., 2013, "Numerical Shape Optimization of a Confined Cavity in Natural Convection Regime," *Computers and Fluids,* **75**, 11-21.
https://doi.org/10.1016/j.compfluid.2012.12.006

Aydin O. and Pop, I., 2007, "Natural Convection in a Differentially Heated Enclosure Filled with a Micropolar Fluid," *International Journal of Thermal Science*, **46**, 963-969.
https://doi.org/10.1016/j.ijthermalsci.2006.11.018

Bejan, A., 2004, "Convection heat transfer," Wiley, New York.

Bénard, H., 1900, "Etude Expérimentale des Courants de Convection dans une Nappe Liquide.- Régime Permanent : Tourbillons Cellulaires," *Journal de Physique Théorique et Appliquée*, **9** (1), 513-524.
https://doi.org/10.1051/jphystap:0190100100025400

Global Digital Central
ISSN: 2151-8629

Bouzidi, M., d'Humières, D. and Lallemand, P., 2001, "Lattice Boltzmann Equation on a Two-Dimensional Rectangular Grid," *Journal of Computational Physics,* **172**, 704-717.
https://doi.org/10.1006/jcph.2001.6850

Calgagni, F., Marsili, F. and Paroncini, M., 2005, "Natural Convective Heat Transfer in Square Enclosures Heated from Below," Applied Thermal Engineering, **25**, 2522-2531.
https://doi.org/10.1016/j.applthermaleng.2004.11.032

De Vahl Davis, G., 1983, "Natural Convection of Air in a Square Cavity: A Bench-Mark Numerical Solution," *International Journal for Numerical Methods in Fluids,* **33**, 249-264.
https://doi.org/10.1002/fld.1650030305

Eringen, A. C., 1966, "Theory of Micropolar Fluids," *Journal of Mathematics and Mechanics,* **16**, 1-18.
http://www.jstor.org/stable/24901466

Eringen, A. C., 1972, "Theory of Thermomicrofluidics," *Journal of Mathematical Analysis and Applications,* 1972, 480-496.
https://doi.org/10.1016/0022-247X(72)90106-0

El Abdallaoui, M., Hasnaoui, M. and Amahmid, A., 2014, "Lattice-Boltzmann Modeling of Natural Convection Between a Square Outer Cylinder and an Inner Isosceles Triangular Heating Body," *Numerical Heat Transfer Part A,* **33**, 1076-1096.
http://dx.doi.org/10.1080/10407782.2014.894398

El Abdallaoui, M., Hasnaoui, M. and Amahmid, A., 2015, "Numerical Simulation of Natural Convection Between a Decentered Triangular Heating Cylinder and a Square Outer Cylinder Filled with a Pure Fluid or a Nanofluid Using the Lattice Boltzmann Method," *Powder Technology,* **277**, 193-205.
https://doi.org/10.1016/j.powtec.2015.02.042

Guo, Y., Bennacer, R., Ameziani, D. E. and Bouzidi, M., 2010, "Simulation of Mixed Convection in Slender Rectangular Cavity with Lattice Boltzmann Method," *International Journal of Numerical Methods for Heat and Fluid Flow,* **20**, 130-148.
https://doi.org/10.1108/09615531011008163

Guo, Z. and Zhao, T. S., 2005, "A Lattice Boltzmann Model for Convection Heat Transfer in Porous Media," *Numerical Heat Transfer Part B,* **47**, 157-177.
http://dx.doi.org/10.1080/10407790590883405

Hasnaoui, M., Vasseur, P. and Bilgen, E., 1992, "Natural Convection in a Rectangular Enclosure with Adiabatic Fin Attached on the Heated Wall," Wärme Stoffübertrag., **27**, 357-368.
https://doi.org/10.1007/BF01600025

Hoyt, J. W. and Fabula, A. G., 1964, "The Effect of Additives on Fluid Friction," *US Naval Ordnance Test Station Report*.
https://doi.org/10.1115/1.3425401

Hsu, T. H. and Chen, C. K., 1996, "Natural Convection of Micropolar Fluids in a Rectangular Enclosure," *International Journal of Engineering Science.,* **40**, 407-415.
https://doi.org/10.1016/0020-7225(95)00103-4

Hsu, T. H., Hsu, P. T. and Tsai, S. Y., 1997, "Natural Convection of Micropolar Fluids in an Enclosure with Heat Sources," *International Journal of Heat and Mass Transfer,* **40**, 7239-4249.
https://doi.org/10.1016/S0017-9310(97)00072-0

Huber, C., Parmigiani, A., Chopard, B., Manga, M. and Bachmann, O., 2008, "Lattice Boltzmann Model for Melting with Natural Convection," *International Journal of Heat and Fluid Flow,* **29**, 1469-1480.
https://doi.org/10.1016/j.ijheatfluidflow.2008.05.002

Jena, S. K. and Bhatacharyya, S. P., 1986, "The effect of Microstructure on the Thermal Convection in a Rectangular Box of Fluid Heated from Below," *International Journal of Engineering Science,* **24**, 69-78.
https://doi.org/10.1016/0020-7225(86)90149-7

Kao, P. H. and Yang, R. J., 2007, "Simulating Oscillatory Flows in Rayleigh–Bénard Convection Using the Lattice Boltzmann Method," *International Journal of Heat and Mass Transfer,* **50**, 3315-3328.
https://doi.org/10.1016/j.ijheatmasstransfer.2007.01.035

Khadiri, A., Amahmid, A., Hasnaoui, M. and Rtibi, A., 2010, "Soret Effect on Double-Diffusive Convection in a Square Porous Cavity Heated and salted from below," *Numerical Heat Transfer Part A*, **57**, 848-868.
http://dx.doi.org/10.1080/10407782.2010.489487

Kimura, S. and Bejan, A., 1983, "The Heatline Visualization of Convective Heat Transfer," *Trans ASME: Journal of Heat Transfer,* **105**, 916-919.
https://doi.org/10.1115/1.3245684

Koriko, O. K. and Animasaun, I. L., 2017, "New Similarity Solution of Micropolar Fluid Flow Problem Over an uhspr in the Presence of Quartic Kind of Autocatalytic Chemical Reaction," *Frontiers in Heat and Mass Transfer,* **8**, 003026.
http://dx.doi.org/10.5098/hmt.8.26

Lallemand, P. and Luo, L. S., 2000, "Theory of the Lattice Boltzmann Method: Dispersion, Dissipation, Isotropy, Galilean Invariance, and Stability", *Physical Review E,* **61**, 6546.
https://doi.org/10.1103/PhysRevE.61.6546

Łukaszewicz, L., 1999, "Micropolar Fluids: Theory and Applications," *Birkhäuser, Basel*.
http://doi.org/10.1007/978-1-4612-0641-5

Mansour, A., Amahmid, A., Hasnaoui, M. and Bourich, M., 2006, "Multiplicity of Solutions Induced by Thermosolutal Convection in a Square Porous Cavity Heated from Below and Submitted to Horizontal Concentration Gradient in the Presence of Soret Effect," *Numerical Heat Transfer Part A,* **49**, 69-94.
http://dx.doi.org/10.1080/10407780500302166

Mezrhab, A., Bouzidi, M. and Lallemand, P., 2004, "Hybrid Lattice-Boltzmann Finite-difference Simulation of Convective Flows," *Computers and Fluids,* **33**, 623-641.
https://doi.org/10.1016/j.compfluid.2003.05.001

Mezrhab, A., Moussaoui, M. A., Jami, M., Naji, H. and Bouzidi, M., 2010, "Double MRT Thermal Lattice Boltzmann Method for Simulating Convective Flows," *Physics Letters A,* **374**, 3499-3507.
https://doi.org/10.1016/j.physleta.2010.06.059

Miroshnichenko, I. V., Sheremet, M. A. and Pop, M. I., 2017, "Natural Convection in a Trapezoidal Cavity Filled with a Micropolar Fluid under the Effect of a Local Heat Source," *International Journal of Mechanical Sciences.,* **120**, 182-189.
https://doi.org/10.1016/j.ijmecsci.2016.11.028

Mliki, B., Abbassi, M. A., Omri, A. and Zeghmati, B., 2016, "Effects of Nanoparticles Brownian Motion in a Linearly/Sinusoidally Heated Cavity with MHD Natural Convection in the Presence of Uniform Heat Generation/Absorption," *Powder Technology,* **295**, pp. 69-83.
https://doi.org/10.1016/j.powtec.2016.03.038

Mohamad, A. A. and Kuzmin, A., 2010, "A Critical Evaluation of Force Term in Lattice Boltzmann Method, Natural Convection Problem," *International Journal of Heat and Mass Transfer,* **53**, 990-996.
https://doi.org/10.1016/j.ijheatmasstransfer.2009.11.014

Nemati, H., Farhadi, M., Sedighi, K., Fattahi, E. and Darzi, A. A. R., 2010, "Lattice Boltzmann Simulation of Nanofluid in Lid-driven Cavity," *International Communication in Heat and Mass Transfer,* **37**, 1528-1534.
https://doi.org/10.1016/j.icheatmasstransfer.2010.08.004

Ostrach, O., 1972, "Natural Convection in Enclosures," *Advances in Heat Transfer,* **8**, 161-227.
https://doi.org/10.1016/S0065-2717(08)70039-X

Pallares, J., Grau, F. X. and Giralt, F., 1999, "Flow Transitions in Laminar Rayleigh–Bénard Convection in a Cubical Cavity at Moderate Rayleigh Numbers," *International Journal of Heat Mass Transfer,* **42**, 753-776.
https://doi.org/10.1016/S0017-9310(98)00192-6

Platten, J. K., Marcoux, M. and Mojtabi, A., 2007, "The Rayleigh–Bénard Problem in Extremely Confined Geometries with and without the Soret Effect," *Comptes Rendus Mécanique,* **335**, 638654.
https://doi.org/10.1016/j.crme.2007.08.011

Qian, Y. H., d'Humières, H. D. and Lallemand, P., 1992, "Lattice BGK Models for Navier-Stokes Equation," *Europhysics. Letters,* **17**, 479-484.
https://doi.org/10.1209/0295-5075/17/6/001

Raji, A., Hasnaoui, M., Firdaous, M. and Ouardi, C., 2013, "Natural Convection Heat Transfer Enhancement in Square Cavity Periodically Cooled from Above," *Numerical Heat Transfer Part A,* **63**, 511-533.
http://dx.doi.org/10.1080/10407782.2013.733248

RamReddy, C. and Pradeepa, T., 2007, "Influence of Convective Boundary Condition on Nonlinear Thermal Convection Flow of a Micropolar Fluid Saturated Porous Medium with Homogeneous-Heterogeneous Reactions," *Frontiers in Heat and Mass Transfer,* **8**, 003006.
http://dx.doi.org/10.5098/hmt.8.6

Saha, S. C., 2011, "Unsteady Natural Convection in a Triangular Enclosure under Isothermal Heating", *Energy and Buildings,* **43**, 695-703.
https://doi.org/10.1016/j.enbuild.2010.11.014

Wu, J. S. and Shao, Y. L., 2004, "Simulation of Lid-Driven Cavity Flows by Parallel Lattice Boltzmann Method Using Multi-Relaxation-Time Scheme," *International Journal of Numerical Methods in Fluids,* **46**, 921-937.
https://doi.org/10.1002/fld.787